CHIN. PHYS. LETT. Vol. 35, No. 8 (2018) 086701

Observation of Atomic Dynamic Behaviors in the Evaporative Cooling by In-Situ Imaging the Plugged Hole of Ultracold Atoms *

Tian-You Gao(高天佑)[1,3], Dong-Fang Zhang(张东方)[1**], Ling-Ran Kong(孔令冉)[1,3], Rui-Zong Li(李睿宗)[1,3], Kai-Jun Jiang(江开军)[1,2**]

[1]*State Key Laboratory of Magnetic Resonance and Atomic and Molecular Physics, Wuhan Institute of Physics and Mathematics, Chinese Academy of Sciences, Wuhan 430071*

[2]*Center for Cold Atom Physics, Chinese Academy of Sciences, Wuhan 430071*

[3]*University of Chinese Academy of Sciences, Beijing 100049*

(Received 20 April 2018)

We experimentally observe the dynamic evolution of atoms in the evaporative cooling, by in-situ imaging the plugged hole of ultracold atoms. Ultracold rubidium atoms confined in a magnetic trap are plugged using a blue-detuned laser beam with a waist of 20 μm at a wavelength of 767 nm. We probe the variation of the atomic temperature and width versus the radio frequency in the evaporative cooling. Both the behaviors are in good agreement with the calculation of the trapping potential dressed by the rf signal above the threshold temperature, while deviating from the calculation near the phase transition. To accurately obtain the atomic width, we use the plugged hole as the reference to optimize the optical imaging system by precisely minimizing the artificial structures due to the defocus effect.

PACS: 67.85.−d, 67.10.Ba, 64.70.fm, 37.10.De DOI: 10.1088/0256-307X/35/8/086701

Ultracold quantum gases have become the common tabletop to study the divergent quantum effects in dilute gases, such as the high precision atomic clock,[1,2] quantum simulation,[3] ultracold chemistry,[4,5] equation of state,[6,7] polaron behavior,[8,9] spin-orbit coupling,[10,11] and p-wave or higher partial wave interaction.[12,13] Evaporative cooling is a prerequisite in cooling atoms into quantum degeneracy. In the radio-frequency (rf) evaporative cooling, atoms with high energy escape from the trap due to the fact that the radio frequency induces spin flip and the remaining atoms rethermalize with the aid of the elastic collision. With decreasing the radio frequency, a larger fraction of atoms will occupy lower energies, which results in a new velocity distribution corresponding to a lower temperature. The microscopic mechanism should be mapped on the macroscopic effects, such as atomic temperature and atomic cloud size. However, while the Bose–Einstein condensate (BEC) has been experimentally realized in alkali atoms[14−16] for tens of years, the dynamic process of atoms in the evaporative cooling is yet to be completely understood. Nowadays, *in-situ* imaging atoms in the trap has become an important technique in exploring quantum behaviors of ultracold quantum gas.[7,17] It can also be an efficient method to probe the dynamic behaviors of atoms in the evaporative cooling.

In this Letter, we experimentally observe the dynamic evolution of atoms in the evaporative cooling, by *in-situ* imaging the plugged hole of ultracold atoms. We plug a blue-detuned laser beam with a waist of 20 μm and a wavelength of 767 nm into the ultracold atoms, forming a compact hole in the atomic cloud, then probe the variation of the atomic temperature and width versus the rf in the evaporative cooling. We also calculate the height and width of the trapping potential dressed by the rf signal, which can become a good reference to understand the atomic dynamics in the evaporative cooling. Both behaviors of atomic temperature and width have a good agreement with the calculation above the threshold temperature, while they deviate from the calculation near the phase transition. To accurately obtain the atomic width, we use the plugged hole as the reference to optimize the optical imaging system by precisely minimizing the artificial structures due to the defocus effect. This work can deepen our understanding of the dynamic process in which the thermal gases are cooled across the phase transition.

Rubidium BEC is produced in an optically plugged magnetic quadrupole trap (OPQT).[18] The experimental setup is shown in Fig. 1. Cold atoms are confined in a magnetic quadrupole trap provided by a pair of magnetic coils. The vacuum pressure of the chamber is 2.0×10^{-11} Torr, and the atomic lifetime in the magnetic trap is about 70 s, which is long enough for the rf evaporative cooling. When the radio frequency is scanned down, the atomic temperature decreases proportionally as the hot atoms are evaporated away by the rf driving spin-flip transition. Ultracold atoms are plugged with a blue-detuned laser beam at a wavelength of 767 nm. Due to the small detuning relative to the resonant wavelength 780 nm, a low power of about 200 mW is sufficient to form a hole, which greatly improves the experimental stability and simplicity. The plugged laser beam is focused with a waist of 20 μm to increase the optical barrier height. A hole appears when the atomic temperature is low enough, which is

*Supported by the National Key Research and Development Program of China under Grant No 2016YFA0301503, the National Natural Science Foundation of China under Grant Nos 11674358 and 11434015, and the Instrument Project of the Chinese Academy of Sciences under Grant No YJKYYQ20170025.

**Corresponding author. Email: zdf0116@wipm.ac.cn; kjjiang@wipm.ac.cn

shown on the left-top side of Fig. 1. The plug beam exactly overlaps the zero point of the magnetic field, suppressing the spin-flip loss by pushing atoms away from approaching the hole. We use the standard absorption imaging method to monitor the hole structure. Atoms in the magnetic trap are in the spin state $|F=1, m_F=-1\rangle$, and are optically pumped to the state $|F=2\rangle$ before being probed.

A collimated resonant probe beam at a wavelength of 780 nm is shined on the atomic cloud. After propagating through cold atoms, the probe beam and the plug beam with orthogonal polarizations are spatially separated by a polarization beam splitter (PBS). Only the probe beam passes through a lens and is detected by the CCD. An optical filter with a bandwidth of 10 nm (band No: Thorlabs-FBH780-10) is inserted in front of the CCD to block stray light away from 780 nm, especially for the plug beam. The imaging system is in the standard 4-f configuration with a magnification factor of 1, where $f = 200$ mm is the focal length of the lens. The spatial resolution is 7.5 μm, which is comparable to the CCD pixel size 6.8 μm.

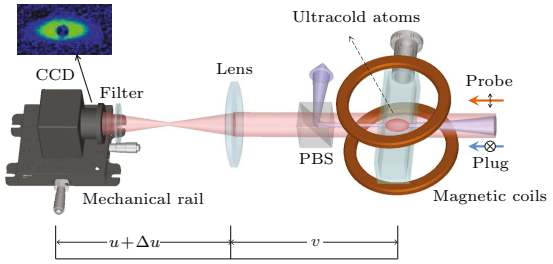

Fig. 1. Schematic of the experimental setup. CCD: charge-coupled device, PBS: polarization beam splitter. The rf signal for the evaporative cooling is not shown for simplicity. The left-top picture shows the image of cold atoms with a plugged hole.

In Fig. 2(a) we show the evolution of the hole when decreasing the atomic temperature. When the rf is scanned down from 3.0 MHz to 1.4 MHz and the atomic temperature decreases from 22.0 μK to 5.6 μK, a hole clearly exists in the atomic cloud. When the radio frequency is 1.0 MHz and the atomic temperature is 1.7 μK, the plug beam splits the atomic cloud into two parts. To quantitatively extract the dynamic information in the evaporative cooling, we empirically fit the optical depth (OD) distribution of atoms with a double-Gaussian function

$$OD(x) = OD_0 + \frac{OD_1}{w_1\sqrt{\pi/2}} \exp\left[-2\left(\frac{x-x_1}{w_1}\right)^2\right] + \frac{OD_2}{w_2\sqrt{\pi/2}} \exp\left[-2\left(\frac{x-x_2}{w_2}\right)^2\right], \quad (1)$$

where the exemplary fitting result for the radio frequency 1.0 MHz is shown in Fig. 2(b), OD_1 and OD_2 are the amplitudes, w_1 and w_2 are the widths of the two Gaussian distributions, respectively. Thus we can obtain the effective width of atoms by defining $w = (w_1 + w_2)/2$.

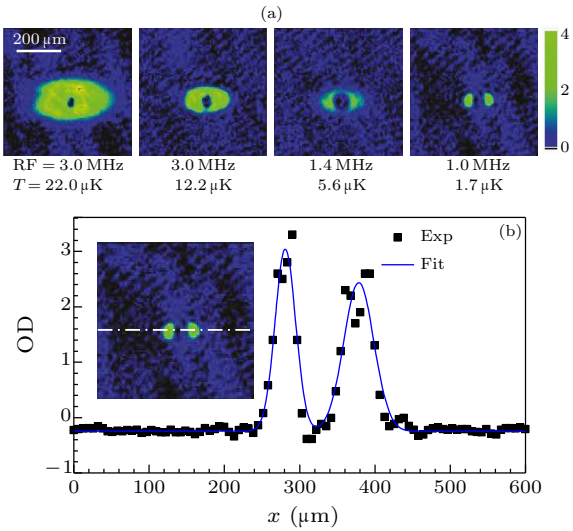

Fig. 2. Evolution of the plugged hole in the evaporative cooling. (a) Atomic images for different radio frequencies. Atomic temperatures are also shown. (b) The optical depth (OD) distribution along the central line of the atomic cloud. The black squares are the experimental results. The blue solid curve is the numerical fitting with a double Gaussian function as Eq. (1). The inset picture is the absorption image for the radio frequency 1.0 MHz and the dot-dashed line denotes the central line of the atomic cloud.

In the evaporative cooling, the magnetic trapping potential created by the magnetic coils does not change, but the total trapping potential including the rf-signal coupling will decrease, which effectively pushes atoms with high energy away from the trap. The temperature and width of atoms are dependent on the height and width of the trapping potential, respectively. We write the trapping potential dressed by the rf signal[19–21]

$$U = -\sqrt{[\mu B'(x^2+y^2+4z^2)^{1/2} - \hbar\omega_{\rm rf}]^2 + (\hbar\Omega_{\rm rf})^2} + U_0 \exp\left[\frac{-2(x^2+z^2)}{d^2}\right] + mgz, \quad (2)$$

where the plug beam is along the y-direction, the gravity is along the z-axis, μ is the magnetic moment of the rubidium atom, B' is the magnetic gradient of the quadrupole field along the radial direction, $\omega_{\rm rf}$ and $\Omega_{\rm rf}$ are the frequency and Rabi frequency of the rf signal, and d is the waist of the optical plug beam. Using our experimental parameters $\Omega_{\rm rf} \approx 2\pi \times 1$ kHz and $d = 20$ μm, we can plot the trapping potential along the x-direction in Fig. 3(a). When the radio frequency is scanned down from 1.5 MHz to 0.6 MHz, the height and width of the trapping potential become smaller, which results in smaller atomic size and lower temperature. The trapping potential is symmetric relative to the central optical barrier. To quantitatively explore the dynamic evolution of cold atoms in the trapping potential, we define two parameters $\Delta x = |x_1 - x_0|$ and $\Delta U = |U_1 - U_0|$, denoting the width and height of the trap, respectively, and Δx and ΔU can be numerically calculated from Eq. (2). The atomic temperature T is determined by the time-of-flight (TOF) method,

and the atomic width w can be extracted as shown in Fig. 2. The numerical calculation and the measured results are both shown in Figs. 3(b) and 3(c). When $\omega_{\rm rf}$ is scanned down, Δx and ΔU both decrease linearly. The atomic width w and temperature T also catch up with this change. The Bose condensate phase transition occurs in the range of $\omega_{\rm rf} = 2\pi \times 0.75\,{\rm MHz}$–$2\pi \times 0.80\,{\rm MHz}$, where the atom numbers are 5.3×10^5 and 3.1×10^5 before and after the phase transition, respectively. We can produce a nearly pure Bose condensate when $\omega_{\rm rf} = 2\pi \times 0.60\,{\rm MHz}$ and $T = 120\,{\rm nK}$. For thermal gases $\omega_{\rm rf} > 2\pi \times 1.0\,{\rm MHz}$, both the behaviors of atomic width and temperature have good agreements with the prediction of Eq. (2).

Several measurements for $T < T_{\rm c}$ are shown in Fig. 3(b) and 3(c). When $\omega_{\rm rf} < 2\pi \times 1.0\,{\rm MHz}$ close to the phase transition, the atom widths are larger than the theoretical predictions and the atomic temperatures are smaller than the calculations. These two behaviors may become signals of the phase transition. We measure the atomic width by fitting the atomic image with the Gaussian distribution like in Fig. 2. Thus the measured width is for the thermal cloud. Below the phase transition, the repulsive interaction between the condensate and the thermal gas increases the size of the thermal component. Our theoretical model of Eq. (2) is only valid for the thermal gas without including the interaction. Thus the deviation of the atomic width from the theoretical curve can be an evidence of the appearance of the condensate. Theoretical works[22–24] have predicted the interaction between the condensate and thermal gases. In experiment, researchers also have observed the increasing size of the thermal gas due to the presence of the condensate in a magnetic trap with the quadrupole Ioffe configuration (QUIC).[25] We measure the atom temperature T using the standard TOF method. The anomalous behavior that the temperature suddenly decreases near the phase transition is consistent to the theoretical prediction[22] and previous experimental observations.[26,27]

It is noted that the aberration will affect the imaging process to some extent. In our imaging system, the focus length of the lens is 200 mm and the diameter is 50.8 mm. We use the software to numerically simulate the spatial resolution. The resolution including the aberration is 8.1 μm, which is slightly larger than that without the aberration 7.5 μm. In Fig. 3(b), the minimum waist radius of the atomic cloud is 17.7 μm. Thus the spatial resolution is smaller than one fourth of the diameter of the atomic cloud for each data in Fig. 3(b). In this case, the aberration should have a negligible effect on our measurement.

The defocus effect has an important effect on the determination of atomic number and temperature as well as the atomic size. To take clear atomic images like in Fig. 2(a) and obtain accurately the atomic width, we need to optimize the optical imaging system because the defocus effect generally produces artificial spatial structures in the obtained images.[28–30] Here we use the plugged hole as the reference to optimize the optical imaging system shown in Fig. 1. Here v and u are fixed and we can precisely change Δu by adjusting the position of the CCD, which is connected on a controllable mechanical rail. When Δu is optimized, the CCD exactly stays in the imaging plane and a perfect circular hole appears in the absorption image as shown on the left top of Fig. 1. If Δu deviates from the optimized value, artificial structures will appear around the hole due to the defocus effect. We can then focus the imaging system by minimizing the artificial structures.

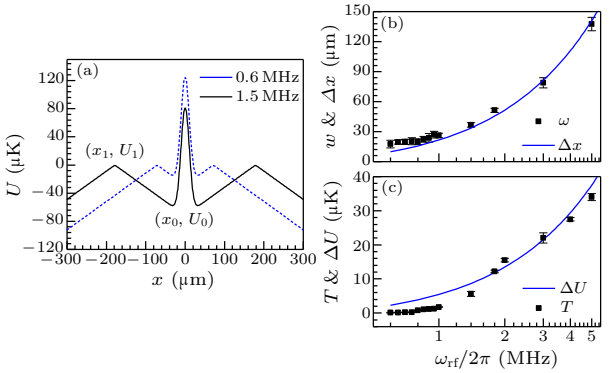

Fig. 3. Variation of atomic width and temperature in the evaporative cooling. (a) The trapping potential dressed by the rf signal. The black solid curve is for $\omega_{\rm rf} = 2\pi \times 1.5\,{\rm MHz}$ and the blue solid curve for $\omega_{\rm rf} = 2\pi \times 0.6\,{\rm MHz}$. Here (x_1, U_1) and (x_0, U_0) indicate the trapping potential maximum and minimum, respectively. (b) The measured atomic width w and the trapping potential width Δx versus $\omega_{\rm rf}$, and Δx is empirically scaled by a factor of 4. The horizontal axis displays logarithmically. (c) The measured atomic temperature T and the trapping potential height ΔU versus $\omega_{\rm rf}$, ΔU is empirically scaled by a factor of 6, w is defined in Eq. (1) and obtained as in Fig. 2, Δx and ΔU are defined in the main text.

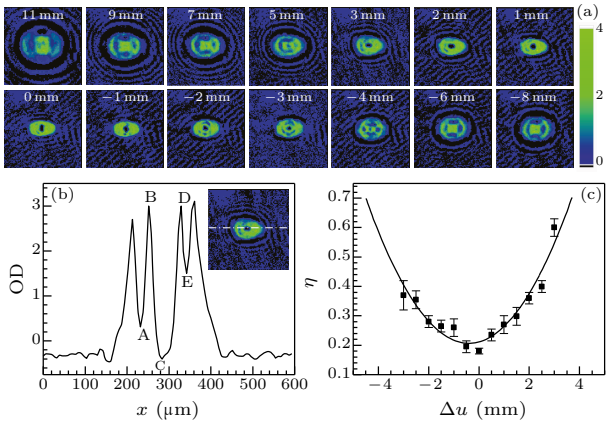

Fig. 4. Optimizing the imaging system when the radio frequency is 1.8 MHz and the atomic temperature is 12.2 μK. (a) Absorption images for 14 different values of Δu. The color bar denotes the optical depth (OD). (b) OD distribution along the center of the atomic cloud indicated by the dot-dashed white line on the inset picture. A, B, C, D, and E denote the points used to define the imaging quality factor η. The inset picture is the absorption image for Δu =3 mm. (c) The imaging quality factor η versus Δu. The error bars denote the standard deviation (SD) of experimental measurements. The solid line is the numerical fitting with a parabolic function.

During optimizing the absorption imaging system,

u and v are first roughly adjusted with $u \sim 2f$ and $v \sim 2f$. When the radio frequency is 1.8 MHz, the atomic temperature is about 12.2 μK. Figure 4(a) shows 14 absorption images with different values of Δu. One specific Δu, which is close to the optimal one, is set as 0 mm. When Δu is large like $\Delta u = 11$ mm, 9 mm, 7 mm, 5 mm, −4 mm, −6 mm or −8 mm, the density distribution in the central area of the atomic cloud deviates strongly away from a hole, indicating that the CCD is severely away from the imaging plane. This phenomenon is similar to that in Ref. [31], where the core of the vortex is filled up due to the strong defocusing effect. When Δu is small like $\Delta u = 3$ mm, 2 mm, 1 mm, 0 mm, −1 mm, −2 mm or −3 mm, a hole clearly exists in the absorption image, but artificial interference fringes appear around the hole more or less. To quantitatively analyze the imaging quality, we plot the column optical depth (OD) through the center of the atomic cloud (like Fig. 4(b)) and define the imaging quality factor as

$$\eta = \frac{(OD_{\rm B} - OD_{\rm A}) + (OD_{\rm D} - OD_{\rm E})}{OD_{\rm B} + OD_{\rm D} - 2OD_{\rm C}}. \quad (3)$$

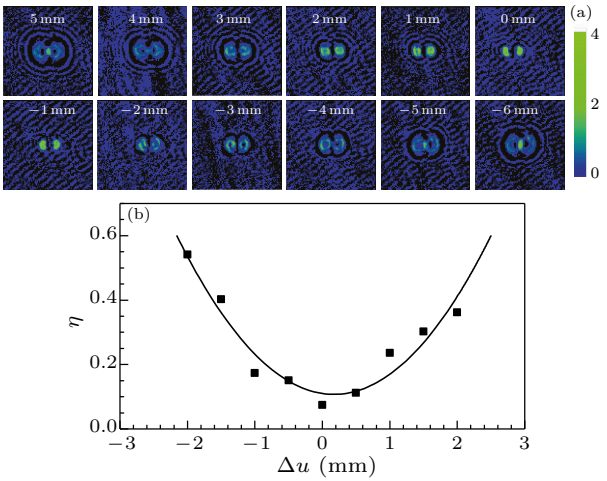

Fig. 5. Optimizing the imaging system when the radio frequency is 1.0 MHz and the atomic temperature is 1.7 μK. (a) Absorption images for 12 different values of Δu. (b) The imaging quality factor η versus Δu. The solid line indicates the numerical fitting with a parabolic function.

When CCD approaches the image plane, two dips denoted by A and E become smaller. Small η indicates a weak defocus effect and vise versa. We plot η in Fig. 4(c) for small values of Δu. Noting that the defocusing effect should be symmetric for small defocusing distances, we use a parabolic function $\eta = a + b(\Delta u + \Delta u_0)^2$ to fit the experimental results, where a and b are the arbitrary fitting parameters. The numerical fitting gives $\Delta u_0 = 0.4(1)$ mm, which means that the optimal value of Δu is −0.4 mm.

In Fig. 5 we also optimize the imaging system using a colder atomic cloud. Figure 5(a) shows 12 absorption images when the radio frequency is 1.0 MHz and the atomic temperature is 1.7 μK. The plug beam splits the atomic cloud into two parts. When Δu is large like $\Delta u = 5$ mm, 4 mm, 3 mm, −3 mm, −4 mm, −5 mm or −6 mm, two artificial holes exist in the two separated atomic clouds. Under these conditions the CCD position is severely away from the optimal one. For small values of Δu in the range from −2 mm to 2 mm, we plot the imaging quality factor η in Fig. 5(b). The parabolic fitting gives $\Delta u_0 = -0.2(1)$ mm, which shifts about 0.6 mm due to the day-to-day mechanical fluctuation.

In conclusion, we have experimentally observed the dynamic evolution of atoms in the evaporative cooling, by *in-situ* imaging the plugged hole of ultracold atoms. We probe the variation of the atomic temperature and width in the rf evaporative cooling. Both the behaviors are in good agreement with the calculation of the trapping potential dressed by the rf signal above the threshold temperature, while they deviate from the calculation near the phase transition. This may become a signal of the phase transition from the thermal gases to the Bose condensate. We use the plugged hole as the reference to optimize the optical imaging system, to accurately obtain the atomic width. The accuracy of positioning the imaging system is less than 1 mm.

We thank Kai Li and Liuyang Cheng for the helpful discussion about the experimental setup.

References

[1] Bloom B J et al 2014 *Nature* **506** 71
[2] Hinkley N et al 2013 *Science* **341** 1215
[3] Bloch I et al 2008 *Rev. Mod. Phys.* **80** 885
[4] Jin D S and Ye J 2012 *Chem. Rev.* **112** 4801
[5] de Miranda M H G et al 2011 *Nat. Phys.* **7** 502
[6] Horikoshi M et al 2010 *Science* **327** 442
[7] Nascimbene S et al 2010 *Nature* **463** 1057
[8] Schirotzek A et al 2009 *Phys. Rev. Lett.* **102** 230402
[9] Nascimbene S et al 2009 *Phys. Rev. Lett.* **103** 170402
[10] Lin Y J et al 2011 *Nature* **471** 83
[11] Peng S et al 2012 *Phys. Rev.* A **86** 063610
[12] Gunter K et al 2005 *Phys. Rev. Lett.* **95** 230401
[13] Peng S G et al 2014 *Phys. Rev. Lett.* **112** 250401
[14] Anderson M H et al 1995 *Science* **269** 198
[15] Davis K B et al 1995 *Phys. Rev. Lett.* **75** 3969
[16] Bradley C C et al 1995 *Phys. Rev. Lett.* **75** 1687
[17] Ho T L and Zhou Q 2010 *Nat. Phys.* **6** 131
[18] Zhang D et al 2016 *Chin. Phys. Lett.* **33** 076701
[19] Davis K B et al 1995 *Phys. Rev. Lett.* **74** 5202
[20] Garraway B M and Perrin H 2016 *J. Phys.* B **49** 172001
[21] Zobay O and Garraway B M 2001 *Phys. Rev. Lett.* **86** 1195
[22] Zhang W et al 2005 *Phys. Rev.* A **72** 053627
[23] Naraschewski M and Stamper-Kurn D M 1998 *Phys. Rev.* A **58** 2423
[24] Liu X J et al 2004 *Phys. Rev.* A **69** 043605
[25] Mishra S R et al 2017 *Pramana* **88** 59
[26] Wang Y Z et al 2003 *Chin. Phys. Lett.* **20** 799
[27] Andrews M R et al 1996 *Science* **273** 84
[28] Choi J et al 2012 *Phys. Rev. Lett.* **109** 125301
[29] Langen T 2013 *Phys. Rev. Lett.* **111** 159601
[30] Choi J et al 2013 *Phys. Rev. Lett.* **111** 159602
[31] Seo S W et al 2014 *J. Korean Phys. Soc.* **64** 53